Z. Phys. B Condensed Matter 60, 1–11 (1985)

Condensed Matter
Zeitschrift für Physik B

Influence of the Acoustic Phonon Scattering Anisotropy on the Distribution Function and the Electronic Transport in *n*-Si

V.V. Mitin
Max-Planck-Institut für Festkörperforschung, Stuttgart, Federal Republic of Germany*

Received February 27, 1985

The Herring-Vogt transformation is ordinarily used in many-valley semiconductors to reduce the ellipsoidal surfaces of constant energy in each valley α to spheres. As a result effective electric and magnetic fields, $\mathbf{E}^*$ and $\mathbf{H}^*$ respectively, are introduced in each valley α. For $\mathbf{E}^* \perp \mathbf{H}^*$ these two fields are the only parameters needed to describe the properties of the electrons in the valley α for isotropic scattering. For that reason and to simplify the Monte Carlo calculations previous authors have mostly introduced the equivalent isotropic acoustic phonon scattering (APS). The present Monte Carlo calculations are performed for *n*-Si at 27 K. It is shown that the electronic properties in valley α (the mean velocity $\mathbf{v}^*$, the mean energy $\bar{\varepsilon}$, the intervalley scattering time τ, etc.) depend on the orientation of the $\mathbf{E}^*$ and $\mathbf{H}^*$ to the principal axes of the valley α, if the APS anisotropy is taken into account. In particularly, τ may changes by one order of magnitude under the rotation of vectors $\mathbf{E}^*$ or $\mathbf{H}^*$. But the dependence of τ on $\bar{\varepsilon}$ is almost universal function, which depends only on the scalar H^*. For a fixed $\bar{\varepsilon}$ the heating of the high energy electrons increases and τ decreases considerably as H^* increases. The negative differential conductivity of *N*-type for $H=0$ and *S*-type for a strong magnetic field are more pronounced for current along [100] axis if the APS anisotropy is taken into account.

1. Introduction

Hot electron phenomena in Si have been extensively studied [1, 2]. Recently increasing interest has been paid to high electric field transport because device miniaturization has led to the necessity of considering electron heating in most semiconducting devices [3–6]. To understand the properties of semiconducting samples and devices it is necessary to solve nonlinear transport equation [1–6]. The Monte Carlo technique is one of the most frequently used methods [7–10] for the solution of the Boltzmann transport equation. This method is now well developed and it is succesfully used for some special orientation of the current $\mathbf{j}$ relative to crystallographic axes in many-valley semiconductors for the case when the magnetic field H is zero [8, 10, 11].

The situation changes drastically if H is present. An additional difficulty is caused not by the magnetic field itself, but by the Hall component [1, 2] of the electric field E_H, which arises in the sample. An additional Sasaki-Shibuya component E_s also arises in the many-valley semiconductor due to the intervalley redistribution of the electrons [1, 2]. These two components are really impossible to separate due to their mutual influence, but it is important that they together form the transverse (to the current) electric field component E_t. The calculation of the galvanomagnetic properties of the many-valley semiconductors in the heating electric field is rather complicated because the total electric field, E, (which includes the applied component E_p as well as transverse component E_t) is in the result for the electron heating. It means that for a semiconductor with λ valleys the distribution functions corresponding to different valleys and the transverse field E_t should be obtained self-consistently, i.e. by solving a system of

* Permanent address: Institute of Semiconductors, Academy of Sciences of the Ukrainian SSR, Kiev, USSR. The research was supported by the Alexander von Humboldt Foundation

$\lambda+1$ equations (λ transport equations and the condition that the transverse current vanishes). The simplest situation with the given $E=E_p$, ($E_t=0$), is normally investigated for many valley semiconductors [9–11] to avoid the self-consistency of the problem. Such a method with given $E=E_p$ may be used at low temperature in n-Si only for $\mathbf{j}/\!/(100)$. For $j/\!/(111)$ and $j/\!/(110)$ the equal population of the equivalent valleys is unstable and new stable states with preferential population of one of the valley and with the transverse field arise [12, 13] in a certain range of the applied field E_p.

There is another possibility to simplify the problem [13, 14]. In n-Si and other materials with ellipsoidal surfaces of constant energy the Herring-Vogt transformation [15] is usually used to transform these surfaces into spherical ones. After this transformation, all valleys become spherical, but instead of one $\mathbf{E}$ and one $\mathbf{H}$ there arise λ effective fields $\mathbf{E}^*$ and λ effective fields $\mathbf{H}^*$, because the transformation is applied in each valley to $\mathbf{E}$ and $\mathbf{H}$ [1, 2, 9, 10, 13, 14] (These effective fields are introduced further by (7)). The transport equation in a separate valley may be solved and dependences of the distribution function and all parameters (such as mean velocity $\bar{\mathbf{v}}^*$, mean energy $\bar{\varepsilon}$, intervalley relaxation time τ and so on) on $\mathbf{E}^*$ and $\mathbf{H}^*$ in the valley may be found. The transverse component E_t may be computed for any orientation of the current relative to the crystallographic axes taking into account the normal phenomenological equation that the transverse current vanishes and calculated dependences of $\bar{\mathbf{v}}^*$, and τ on $\mathbf{E}^*$ and $\mathbf{H}^*$ in a separate valley. This procedure is simple enough. It is described in detail in many publications (see e.g. [1, 2, 12–14]) and it will be briefly discussed in Appendix.

It is necessary to stress that after Herring-Vogt transformation the acoustic phonon scattering (APS) remains anisotropic and it is replaced by the equivalent isotropic APS [9, 10, 12, 13]. Such a replacement is justifiable in the case of the quasi-isotropic electron distribution function (EDF). At low temperature the EDF is essentially anisotropic [12, 14] and this approach fails. The anisotropy of the APS for n-Si was taken into account e.g. in the paper [11] for calculation of the current voltage characteristics for current along (111) and (100) directions at $T \geqq 40$ K, $H=0$. We performed the calculations for $T=27$ K when in addition to that considered in paper [11], scattering on low energy g_1 phonon ($\hbar\omega_{q_1}=12$ meV) is important [16, 9, 12] and APS itself has more influence on the electron distribution function and all characteristics of n-Si).

We apply the Monte Carlo method to n-Si bearing in mind two main goals. First of all we want to investigate the role of the anisotropy of the APS in the previously not considered case, when the (transverse to the current) magnetic field H is present. Secondly we want to present the distribution function, $\bar{\mathbf{v}}^*$, $\bar{\varepsilon}$ and τ as a function of the effective electric, $\mathbf{E}^*$, and magnetic, $\mathbf{H}^*$, fields in a separate valley. These dependences may be used for calculations of the intervalley redistribution, transverse electric field, current and so on [1, 2, 12–14] (an example is given in the Appendix).

2. Definition of the Physical Model

Here we apply the Monte Carlo simulation to n-Si at 27 K. This temperature is chosen for the following reasons: APS determines the electron mobility over a wide range of the electric field E; it is the temperature of liquid neon, which is often used for hot electron experiments; calculations with equivalent APS at 27 K have already been performed [12–14] and it gives us an opportunity to investigate the influence of APS anisotropy.

The transition probability per unit time of an electron going from a state with momentum $\mathbf{p}$ to a state $\mathbf{p}'$ in the same valley many-valley semiconductor is given [15, 17] by the expression

$$P_{L,T}^{\mp}(\mathbf{p},\mathbf{p}') = \pi q^{\mp} F_{L,T}(N_{L,T}+\tfrac{1}{2}\pm\tfrac{1}{2})/V \cdot \delta(\varepsilon(\mathbf{p}')-\varepsilon(\mathbf{p})\pm\hbar u_{L,T}q^{\mp}) \tag{1}$$

$$F_L=(\Xi_d+\Xi_u\cos^2\theta)^2/(u_L\rho),$$

$$F_T=\Xi_u^2\cos^2\theta\sin^2\theta/(u_T\rho)$$

where L and T denote the interaction with longitudinal and transverse acoustic phonon modes. Here P^--refers to absorption and P^+ to emission. ρ is the density of the crystal, V its volume, $u_{L,T}$ the longitudinal and transverse sound velocities.

$$\mathbf{q}^{\mp}=\pm(\mathbf{p}-\mathbf{p}')/\hbar \tag{2}$$

is the wave vector of the absorbed or emitted acoustic phonon. Also

$$N_{L,T}=[\exp(\hbar u_{L,T}q_{L,T}^{\mp}/(kT))-1]^{-1} \tag{3}$$

is the number of phonons, Ξ_d and Ξ_u are two components of the deformation potential tensor [15, 17], θ is the angle between $\mathbf{q}^{\mp}$ and the longitudinal axis of the valley considered, k is the Boltzmann's constant, and T is the temperature.

In the Monte Carlo calculation one must integrate over all possible final states [8, 10] to find the probability $W_{L,T}^{\mp}$ of scattering from the state $\mathbf{p}$ to all others. To perform this integration it is convenient

to integrate over $\mathbf{q}^{\mp}$ and to use polar coordinates with the polar axis along the principal axis of the valley:

$$W_{L,T}^{\mp}=\frac{V}{(2\pi)^3}\int_0^{\pi}\sin\theta\,d\theta\int_0^{2\pi}d\phi\int_0^{\infty}(q^{\mp})^2\,dq^{\mp}\,P_{L,T}^{\mp}(\mathbf{p},\mathbf{p}').$$

After integration over $q^{\mp}$ we have

$$W_{L,T}^{\mp}=m_t/h^2\int_{-1}^{+1}d(\cos\theta)\int_0^{2\pi}d\phi(q_{L,T}^{\mp})^2\cdot F_{L,T}\frac{N(q_{L,T}^{\mp})+\frac{1}{2}\pm\frac{1}{2}}{1-\beta\cos^2\theta} \tag{4}$$

where $\beta=1-m_t/m_1$,

$$q_{L,T}^{\mp}=\pm\frac{2m_t u_{L,T}}{\hbar(1-\beta\cos^2\theta)}\left[\left(\frac{2\varepsilon}{m_t u_{L,T}^2}\right)^{\frac{1}{2}}\cdot\frac{m_t\cos\alpha\cos\theta+m_1\sin\alpha\sin\theta\cos\phi}{m_1(1-\beta\cos^2\alpha)^{\frac{1}{2}}}-1\right] \tag{5}$$

is the wave vector of the phonon involved in scattering an electron of energy ε, α is the angle between $\mathbf{p}$ and the longitudinal axis of the valley considered, and θ and ϕ are directional angles of the vector $\mathbf{q}_{L,T}^{\mp}$. Here $1/m_1$ and $1/m_t$ are the longitudinal and transverse components of the inverse effective mass tensor.

It easy to see that the $W_{L,T}^{\mp}$ depend not only on the energy of the electrons ε, but also on the angle α between $\mathbf{p}$ and the longitudinal axis. Even with an isotropic approximation for crystal property, when $\Xi_u=0$ and only longitudinal acoustic phonon modes are important ($W_T^{\mp}=0$), the dependence of $W_L^{\mp}$ on α remains as in (4, 5) and it arises from the δ-function in (1). This dependence was previously also neglected by introduction of the equivalent isotropic APS [9, 10, 12]. It is necessary to stress that APS is inelastic here.

For the calculations we chose $u_L=9.1\cdot10^5$ cm/s, $u_T=5.38\cdot10^5$ cm/s, $\rho=2.33$ gm/cm^3, $m_1=0.9163\,m_0$, $m_t=0.1905\,m_0$ [9, 17–19], where m_0 is the free electron mass. There is a range of values of Ξ_u and Ξ_d in the literature [18] and we chose $\Xi_u=9.1$ eV, $\Xi_d=2$ eV because these are the most frequently cited values [18] and also because they give the same low electric field limit for the mobility as in paper [9, 12, 13] with equivalent isotropic APS.

Figure 1 shows the dependence of $W_{L,T}^{\mp}$ on the electron energy ε. W_L^- is presented for $\alpha=0$ and $\alpha=90°$, but $W_T^{\mp}$ and W_L^+ only for $\alpha=90°$, because the α dependences of these three scattering probabilities are weak. In the Monte Carlo simulation the α dependence of the $W_T^{\mp}$ and W_L^+ are not taken into account because control computations with the

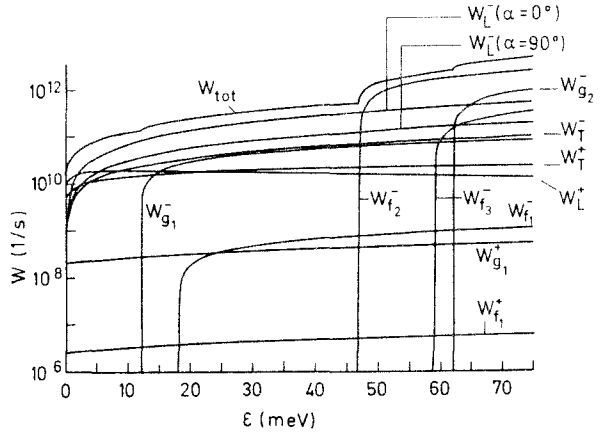

Fig. 1. Energy dependence of the probability of the total electron scattering rate W_{tot} and of the partial probabilities due to emission W^- and adsorption W^+ of longitudinal $W_L^{\mp}$ and transverse $W_T^{\mp}$ acoustic phonons and g_i- and f_i-intervalley phonons $W_{g_i,f_i}^{\mp}$

$W_T^{\mp}(\alpha)$ and $W_L^+(\alpha)$ show negligible deviation from the chosen approach. (The dependences of W_L^+ and $W_T^{\mp}$ on α are not essential, not only because they are small, but also because these three probabilities themselves are small in comparison with W_L^- (Fig. 1)). The α dependence of W_L^- is taken in account. For all $W_{L,T}^{\mp}$ the anisotropy of APS taken into account when the angles θ and ϕ are determined on the basis of the integrand in equation (4) by the ordinary rejection technique [8–10, 13]. For example random θ and ϕ are generated and $q_{L,T}^{\mp}$ is calculated as unphysical, if $q_{L,T}^{\mp}<0$, and a new set of θ and ϕ are generated until $q_{L,T}^{\mp}>0$. Then a new random number r is generated. The $q_{L,T}^{\mp}$ is accepted only if for the considered ε and α the product of r and the maximum value of integrand in (4) is smaller than the value of the integrand for this $q_{L,T}^{\mp}$. The $q_{L,T}^{\mp}$ is rejected in the opposite case and the procedure is repeated from the very beginning, i.e. a new set of θ and ϕ is generated. After the wave vector $\mathbf{q}_{L,T}^{\mp}$ of the phonon involved on the process (5) is found, the final state momentum $\mathbf{p}'$ is calculated from (2). It is necessary to note that for a high electron energy the energy $\hbar u_{L,T}q_{L,T}^-$ of the emmited acoustic phonons is not small in comparison with kT, but may even be considerably larger than kT ($\hbar u_{L,T}q_{L,T}^-$ is of the order of $(mu_{L,T}^2\varepsilon)^{\frac{1}{2}}$), i.e. APS became essentially inelastic for a high electron energy.

In addition to APS we take into account the emission of g_1- and g_2-phonons with energies $\hbar\omega_{g_1}=12$ meV and $\hbar\omega_{g_2}=62$ meV, and of f_1-, f_2- and f_3-phonons – $\hbar\omega_{f_1}=18$ meV, $\hbar\omega_{f_2}=47$ meV, $\hbar\omega_{f_3}=59$ meV. The absorption of g_1- and f_1-phonons is

also included, but the probability of absorption of high energy f- and g-phonons is exponentially small at this temperature. The energy dependence of the probabilities $W_{g1}^{\mp}$, W_{g2}^{-}, $W_{f1}^{\mp}$, $W_{f2,f3}^{-}$ are shown in Fig. 1. (It is necessary to stress that an electron may scatter into one of the four valleys on the other $\langle 100\rangle$ axes and this is taken into account by the factor 4 in the $W_{f1}^{\mp}$, $W_{f2,f3}^{-}$ in Fig. 1). The coupling constants for these five phonons were chosen to be $0.65\cdot10^8$ eV/cm, $7.5\cdot10^8$ eV/cm, $0.0474\cdot10^8$ eV/cm, $4.3\cdot10^8$ eV/cm and $2\cdot10^8$ eV/cm respectively. These constants were discussed in detail in papers [9, 12, 13, 16]. We just note here that the forbidden low energy g_1- and f_1-phonons are included in calculations with small probabilities compared with the three allowed high energy phonons. The f_1-scattering has no influence at all on the distribution function due to small probability and it is included in the calculation only to obtain the correct intervalley scattering time [12, 13] at weak electric field, where scattering by f_2- and f_3-phonons is exponentially small. Scattering by f_1- and g_1-phonons, forbidden by the selection rules must be anisotropic [13, 20]. Here it is taken as isotropic, not only because it was done so in previous publications [9, 10, 12–14, 16], but also because the momentum scattering is controlled in the main by APS up to $\varepsilon = 47$ meV (see in Fig. 1 the probability of total scattering W_{tot}, which represents the sum over all the scattering mechanisms that have been considered).

The electron was assumed to be in the same valley after f-scattering and it provides the opportunity to perform independent calculations in each valley of n-Si. To control the possible error we carried out calculations with an electric field of up to 500 V/cm including all valleys of n-Si. The result, however, was the same reflecting the fact that f_1-scattering has no influence on the distribution function. The f_2- and f_3-phonon scatter the electron into the valley of interest at the energy ε, which is small in comparison with $\hbar\omega_{f_2}$, both after scattering through another valley and in the adopted procedure, where the electron remains in the same valley. The g-scattering is effectively an intravalley scattering, because two valleys in the same axis $\langle 100\rangle$ are not distinguished and all quantites remain the same in both valleys.

The calculations are performed in the presence of an electric field E and a transverse magnetic field H. We use the Herring-Vogt transformation [10, 15], which reduces the ellipsoidal equienergetic surfaces to spheres

$$p_{x,y}^* = (m/m_t)^{\frac{1}{2}} \cdot p_{x,y},$$
$$p_z^* = (m/m_1)^{\frac{1}{2}} p_z, \qquad m = (m_t^2 m_1)^{\frac{1}{3}}. \tag{6}$$

Here $\mathbf{p}^*$ is the transformed wave vector in the frame centered at the bottom of the valley α with the z axis along the longitudinal axis. After applying this transformation to $\mathbf{E}$ and $\mathbf{H}$, the effective electric field $\mathbf{E}^*$ and magnetic field $\mathbf{H}^*$ in valley α are introduced:

$$E_{x,y}^* = (m/m_t)^{\frac{1}{2}} \cdot E_{x,y}, \qquad E_z^* = (m/m_1)^{\frac{1}{2}} \cdot E_z$$
$$H_{x,y}^* = H_{x,y} m/(m_t m_1)^{\frac{1}{2}}, \qquad H_z^* = H_z m/m_t. \tag{7}$$

The transformation (7) preserves the orthogonality of the electric and magnetic fields ($\mathbf{E}^*\mathbf{H}^* \equiv \mathbf{EH}$) and for isotropic scattering the fields E^* and H^* characterize all properties of the electrons in valley α [12–14]. Here for anisotropic APS the dependence on the orientation of $\mathbf{E}^*$ and $\mathbf{H}^*$ relative to the longitudinal axis of valley α remains essential.

After the transformations (6, 7) the equation of motion of an electron with the isotropic effective mass [21] m was used in the Monte Carlo calculations. The nonparabolicity is not taken into account, because it has an influence on $\varepsilon(\mathbf{p})$ relation and on probabilities of scattering only for the energies larger than 0.1 eV [10].

3. Results and Discussion

For each effective field E^* and H^* in the valley considered we calculated:

1. the EDF $f(\varepsilon, \cos\theta_1, \phi_1)$, where θ_1 and ϕ_1 are the polar and azimuthal angles of the spherical coordinate system;

2. the reciprocal intervalley relaxation time τ^{-1} representing the transfer of an electron from the valley under consideration to four other valleys on different $\langle 100\rangle$ axes due to interaction with f_1-phonons (τ_1^{-1}) and with $f_2 + f_3$-phonons (τ_2^{-1});

3. the mean energy of the electrons $\bar{\varepsilon}$;

4. the two components of the mean velocity $\bar{\mathbf{v}}^*$ of the electrons, namely, the components $\bar{v}_{\parallel}^*$ along the effective electric field $\mathbf{E}^*$ and $\bar{v}_{\perp}^*$ in the direction $\mathbf{E}^* \times \mathbf{H}^*$ ($\bar{\mathbf{v}}^*$ is really the current density calculated for one electron in the valley under consideration). The Herring-Vogt transformation for the velocity in the α-valley has the form

$$v_{x,y}^* = (m_t/m)^{\frac{1}{2}} \cdot v_{x,y}, \qquad v_z^* = (m_1/m)^{\frac{1}{2}} \cdot v_z. \tag{8}$$

In all cases considered the $\bar{\mathbf{v}}^*$ component along H^* is zero. The electric field E^* is in the range 10 V/cm to $3\cdot10^3$ V/cm. For $H = 0$ we performed calculations for smaller electric fields to see if the Boltzmann's equilibrium EDF is obtained. In this case the rate of absorption and emission of the g_1- as well as f_1 phonons were equal and also the low electric field

mobility $\mu \simeq 1.1 \cdot 10^5\ \mathrm{cm^2/V \cdot s}$ coincides with previous calculations [12, 13], with experiment [22] and is close to the simple estimation on the basis of expression $\mu = e\langle\tau\rangle/m$, where the average scattering time $\langle\tau\rangle$ was obtained from the simulations.

If **H** is directed along ⟨100⟩, then for two valleys this direction coincides with the longitudinal axis and $H^{*(1)} = Hm/m_t$, but for the other four valleys $H^{*(2)} = Hm/(m_1 m_t)^{\frac{1}{2}}$. These two effective magnetic fields differ by the factor $(m_1/m_t)^{\frac{1}{2}} = 2.19$. This factor is chosen to determine the interval between four values of H^*, namely the calculations are performed for $H^* = 0.27$ T, 0.6, 1.31, and 2.87 T. It is necessary however to distinguish between the cases when **H** is parallel and perpendicular to the longitudinal axis of the valley considered because of scattering anisotropy.

We first deal with the case of **H** parallel to transverse axis with the electric field rotated in the perpendicular plane between the longitudinal axis ($\beta = 0$) and another transverse axis ($\beta = 90°$) of the valley. In the figures presented here the dashed curves show the results for $\beta = 0$ the dot-dashed curves $\beta = 90°$ and for comparison the solid curves show the results for the case of isotropic APS (as in previous publications [9, 12–14]). We also performed calculations for $\beta = 15°$, 30°, 45° and 60°, where β is the angle between **E** and the longitudinal axis of the valley. Results for $\beta = 60°$ and even for $\beta = 45°$ are close to those $\beta = 90°$. This is because $m_1 \gg m_t$ and the angle β^* between the effective field **E*** and the longitudinal axis given by

$$\cos\beta^* = \cos\beta[m_t/(m \cdot (1 - \cos^2\beta(1 - m_t/m_1))^{\frac{1}{2}})]$$

is larger than the angle β. So that **E***, which really determines the direction of the electron accelaration, is almost normal to longitudinal axis. For $\beta = 30°$ the results are generally very close to solid lines, and, naturally, the results for $\beta = 15°$ are between the dashed and the solid lines.

We must stress that for $\beta \neq 0$, 90° a component $\bar{v}_\perp^*$ perpendicular to **E*** appears even for $H = 0$, caused by the scattering anisotropy. This component is most essential in a weak electric field, when APS is the only mechanism, and decreases when E^* increases. For example, for $\beta = 60°$, 45° and 30° the ratio $\bar{v}_\perp^*/\bar{v}_\parallel^*$ decrease from 0.13, 0.20 and 0.26 at weak E^* to 0.1, 0.14 and 0.20, respectively at 300 V/cm.

Figure 2 shows the dependence of $\bar{v}_\parallel^*$ and $\bar{v}_\perp^*$ on E^*, and Fig. 3 the dependence of $\bar{\varepsilon}$ on E^*. Anisotropy of $\bar{v}^*$ and $\bar{\varepsilon}$, i.e. the dependence of these values on the direction of **E***, arises when the APS anisotropy is taken into account. $\bar{v}_\parallel^*$ for $\beta = 90°$ and $\beta = 0$ differ by a factor 1.6 for $H = 0$ and 2.2 in the magnetic fields.

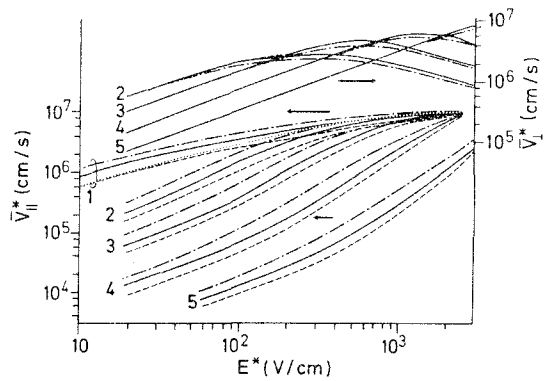

Fig. 2. Dependences of $\bar{v}_\parallel^*$ and $\bar{v}_\perp^*$ vs E^* for **H** parallel to the transverse axis of the valley considered. For $H^* = 0$(1), 0.27(2), 0.6(3), 1.3(4), and 2.87 T(5) in *n*-Si at 27 K for different angle, β, between electric field E and longitudinal axis of the valley. $-\cdot-\beta = 90°$, $-\,-\,-\beta = 0$, ——— calculations using equivalent isotropic APS, ·····-dependence of $\bar{v}^*(E_\parallel^*)$ for $H^* = 0.6$ T, $\beta = 90°$ (for this line the abscissa is $E_\parallel^*$ and the ordinate is $\bar{v}^*$)

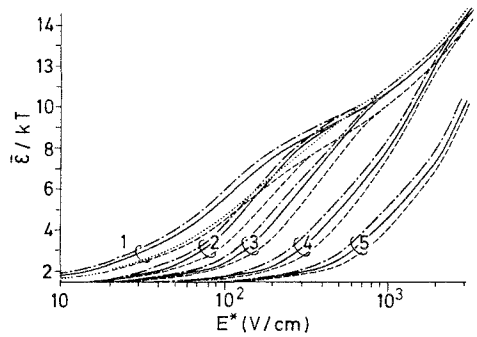

Fig. 3. Dependence of $\bar{\varepsilon}$ vs E^* for the same cases as in Fig. 2

The increase in $\bar{\varepsilon}$ and $v_\parallel^*$ (Fig. 2, 3) is controlled mainly by APS (here $v_\parallel^*$ is proportional [1, 2, 10] to $(E^*)^{\frac{1}{2}}$) up to 200 V/cm at $H = 0$. The increase in $\bar{\varepsilon}$ is considerably slower from 200 V/cm up to 1,000 V/cm, because the emmision of the high energy f_2- and then g_2- and f_3-phonons becomes important in the electron energy relaxation. At a still larger E^* the increase of $\bar{\varepsilon}$ with E^* becames stronger, because in high electric field even high energy phonon emission loses its importance.

This can be seen from Fig. 4, which shows the isotropic part of the EDF

$$f_0(\varepsilon) = \sum_{\mathbf{p}^*} f(\mathbf{p}^*)\,\delta(\varepsilon - \varepsilon_{\mathbf{p}^*}) / \sum_{\mathbf{p}^*} \delta(\varepsilon - \varepsilon_{\mathbf{p}^*}), \tag{9}$$

normalized to one electron, i.e.

$$2\sum_{\mathbf{p}^*} f(\mathbf{p}^*) \equiv \int_0^\infty g(\varepsilon) f_0(\varepsilon)\, d\varepsilon = 1. \tag{10}$$

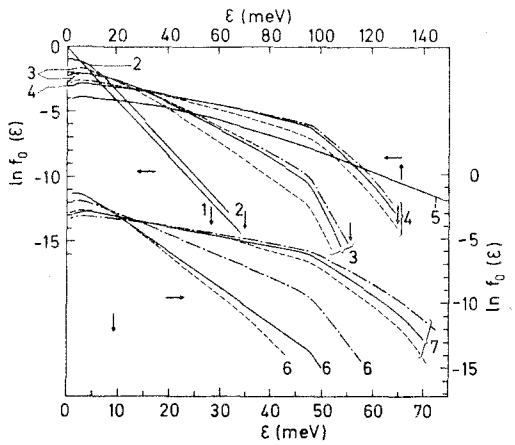

Fig. 4. Isotropic part of the EDF vs ε. $H=0$, $E^*\to 0$ (1), $E^*=10$ V/cm (2), 60 (3), 200 (4), 3,000 V/cm (5); $H^*=0.6$ T, E^* $E^*=100$ V/cm (6), 400 V/cm (7). $-\cdot-\cdot-$ $\beta=90°$, $---$ $\beta=0$, ——— calculations using equivalent APS

Here

$$g(\varepsilon)=2\sum_{\mathbf{p}^*}\delta(\varepsilon-\varepsilon_{\mathbf{p}^*})\equiv(2m^3\varepsilon)^{\frac{1}{2}}/(\pi^2\hbar^3) \tag{11}$$

is the density of electron states at ε.

At weak E^* (for $H=0$ this is $E^*\lesssim 0.5$ V/cm) $f_0(\varepsilon)$ coincides (curve 1) with the equilibrium one: $f_0(\varepsilon)=C\exp(-\varepsilon/kT)$, where C is the normalization constant, which satisfies the equation (10). When E^* increases, the main effect is on the low energy part of $f_0(\varepsilon)$ (curve 2) and at higher energy $f_0(\varepsilon)$ has approximatly the same slope as at $E^*\to 0$. The EDF $f_0(\varepsilon)$ have the pecularity that for $\varepsilon>\hbar\omega_{f_2}$ the slope is larger than in the equilibrium case (curve 3) up to $\simeq 200$ V/cm. It means that the characteristic "temperature" of the electrons in this energy range is less [13] than T, because the EDF here is determined mainly by the emission of high energy f_2-phonons and

$$-\frac{d\ln f_0(\varepsilon)}{d\varepsilon}=\frac{1}{eE^*1(\varepsilon)}>\frac{1}{kT}, \tag{12}$$

where $1(\varepsilon)=v_{\|}(\varepsilon)/W_{\mathrm{tot}}(\varepsilon)$ is the mean free path of electron with energy ε. Of course, for still larger energies the equilibrium slope $1/kT$ will be achived, when the number of electrons coming to a given energy due to phonon absorption will be more than the number arriving due to accelaration in the electric field (12).

For high E^*, $f_0(\varepsilon)$ decreases slowly up to high energies (curve 5: for this curve use the upper energy scale).

Let us now discuss the dependences in a magnetic field. All H^* considered here are classically strong for weak E^*. In our notation a strong magnetic field means $\bar{v}_{\perp}^*>\bar{v}_{\|}^*$, and weak $\bar{v}_{\perp}^*<\bar{v}_{\|}^*$. This definition is normally used for estimation on average, but really it is necessary to take into consideration the energy dependence of the scattering probability. If

$$\frac{eH^*}{cmW_{\mathrm{tot}}(\varepsilon)}<1 \tag{13}$$

the magnetic field H^* is weak for electrons with energy ε. In our case (Fig. 1) $W_{\mathrm{tot}}(\varepsilon)$ increases one order of magnitude up to $\hbar\omega_{g_1}$, then additionally half an order up to $\hbar\omega_{f_2}$ and one order more up to $\varepsilon=75$ meV. For $H^*=2.87$ T, 1.3, 0.6 and 0.27 T the inequality (13) holds for energies $\varepsilon>52$ meV, 48, 35 and 8 meV, respectively (the temperature $T=27$ K corresponds to 2.32 meV). It means that for high energy electron the magnetic fields are weak even at weak E^*. When E^* increases, the number of high energy electrons increases and for each H^* it is possible to reach E^*, when H^* become weak for most electrons and $\bar{v}_{\perp}^*<\bar{v}_{\|}^*$.

From Fig. 2 it is possible to see that at weak E^* $\bar{v}_{\perp}^*$ decrease like $1/H^*$ and $\bar{v}_{\|}^*$ like $1/H^{*2}$, as it must be in the strong magnetic field region [1, 23]. Secondly, $\bar{v}_{\perp}^*$ in the weak E^* region do not depend on the direction of $\mathbf{E}^*$, while $\bar{v}_{\|}^*$ depends on it essentially. It is connected with the fact that in a strong H^* the Boltzmann equation can be solved by iteration on $1/H$. In the zeroth oder approximation the collision term is neglected and the equation has the simple form

$$\left|\mathbf{E}^*+\frac{1}{c}(\mathbf{v}^*\times\mathbf{H}^*)\right|\frac{\partial}{\partial\mathbf{p}^*}f(\mathbf{p}^*)=0 \tag{14}$$

where c is speed of light.

If the $f(p^*)$ is written as

$$f(\mathbf{p}^*)=f_0(\varepsilon)+f_1(\mathbf{p}^*) \tag{15}$$

where $f_0(\varepsilon)$ is the isotropic (9) term and $f_1(\mathbf{p}^*)$ is the anisotropic term [14], without any assumption about the form of $f_1(\mathbf{p})$ one can easily obtain from (14)

$$f_1(\mathbf{p}^*)=-\frac{\mathbf{p}^*(\mathbf{E}^*\times\mathbf{H}^*)c}{H^{*2}}\frac{\partial f_0(\varepsilon)}{\partial\varepsilon}. \tag{16}$$

After substitution of (15), (16) in (14) the terms proportional to $(H^*)^0$ vanish and the term $\sim 1/H^*$ must be included in the first order approximation, where scattering is taken into account. To determine the current, it is not necessary to solve the equation for $f_0(\varepsilon)$ because from (15), (16), (10) one has

$$\bar{\mathbf{v}}^*=2\sum_{\mathbf{p}^*}\mathbf{v}^*f(\mathbf{p}^*)\equiv\frac{c(\mathbf{E}^*\times\mathbf{H}^*)}{H^{*2}}, \tag{17}$$

i.e. $\bar{v}^*$ is directed along the vector $(\mathbf{E}^* \times \mathbf{H}^*)$ (that is why it coincides with $\bar{v}_\perp^*$) and it is proportional to E^* and to $1/H^*$. This is the nondissipative component of the current $(\mathbf{E}^* \cdot \bar{\mathbf{v}}^* = 0)$ and it does not depend on the scattering. The dissipative current $(\bar{v}_\parallel^*)$ is obtained in the first order approximation in $1/H^*$ and in contrast to (17) it is $\sim 1/H^{*2}$.

The linear dependence of $\bar{v}_\perp^*$ on E^* holds in the range $\bar{v}_\perp^* > \bar{v}_\parallel^*$, and here $\bar{v}_\parallel^*$ superline function of E^*. In the vicinity of $\bar{v}_\perp^* = \bar{v}_\parallel^*$, $\bar{v}_\perp^*$ reaches its maximal value then decreases with increasing E^* and $\bar{v}_\parallel^*$ becomes a sublinear function of E^*. In the last region of E^* the magnetic field is effectively small $(\bar{v}_\perp^* < \bar{v}_\parallel^*)$.

The dependence of $\bar{\varepsilon}$ on E^* is more abrupt in stronger magnetic field (Fig. 3) and the difference between EDF for $\beta = 0$ and $\beta = 90$ in the magnetic field is also larger (curve 6, 7 in Fig. 4) than for $H = 0$. There is one more peculiarity in the dependence of $\bar{\varepsilon}$ on E^*. For $H = 0$ the solid curve is considerably closer to the dot-dashed curve for $\beta = 90$ than the dashed one, but in the strong magnetic field region, at least for weak heating E^*, where $\bar{\varepsilon}$ only slightly exceeds $\frac{3}{2}kT$, it is closer to dashed curve for $\beta = 0$.

In the range of high E^*, where H^* become effectively small, $\bar{v}_\parallel^*$ and $\bar{\varepsilon}$ tend to the corresponding curves for $H = 0$ (Fig. 2, 3). Because the influence of H^* on the electron properties decreases when E^* increases.

The quantities $\bar{v}^*$ and $\bar{\varepsilon}$ on Figs. 2 and 3 are plotted against the field E^*, which includes, of course, both components of the $\mathbf{E}^*$: the applied (parallel to the current) component $E_\parallel^*$ and the Hall (perpendicular to the current) one. It easy to calculate the component $E_\parallel^*$:

$$E_\parallel^* = E^*/(1 + (\bar{v}_\perp^*/\bar{v}_\parallel^*)^2)^{\frac{1}{2}} \tag{18}$$

and present the dependences of $\bar{v}^* = (\bar{v}_\parallel^{*2} + \bar{v}_\perp^{*2})^{\frac{1}{2}}$ and $\bar{\varepsilon}$ on $E_\parallel^*$. The first dependence is the current-voltage characteristic of a one valley semiconductor and the second is the dependence of the mean energy on the applied electric field. Of course for $H = 0$ these dependences coincide with $\bar{v}^*(E_\parallel^*)$ and $\bar{\varepsilon}(E^*)$ for each of the three cases presented in Figs. 2 and 3. It is necessary to stress that $v^*(E^*)$ is the current voltage characteristics of one valley. It has nothing in common with the current voltage characteristic of n-Si because the last case requeres taking into account contribution from all valleys. This contribution is proportional to the product of $\bar{\mathbf{v}}^*$ and τ, because the partial concentration of the electrons in a valley is proportional to intervalley scattering time, τ, in this valley (see Appendix).

In the case of effective APS, the dependence of $\bar{v}^*$ on $E_\parallel^*$ for all H^* considered is very close to the solid line 1 in Fig. 2 for $H = 0$, because the differene is only due to magnetoresistance, which is small. (For $\mathbf{E} \to 0$, when the APS predominate, the magnetoresistance is $< 12\%$. It decreases when E^* increases [1, 2]. But the accuracy of the Monte Carlo method here is of the order of 10%, because this method convergences only slowly [7, 10], and increasing accuracy requires a large increases of computer time).

When APS anisotropy is taken into account, the dependences of $\bar{v}^*$, and $\bar{\varepsilon}$, on $E_\parallel^*$ for each magnetic field tends to the corresponding dependences for $H = 0$ in a high electric field, where H^* becomes weak. For $H^* = 0.27$ T this realised at $E_\parallel^* > 500$ V/cm, for $H^* = 0.6$ T at $E^* > 1{,}000$ V/cm. For weak $E_\parallel^*$, where H^* is strong, this is reversed. The curves for $\beta = 90°$ tend to the $\beta = 0°$ $H = 0$ and curves for $\beta = 0°$ to $\beta = 90°$ for $H = 0$, as is shown by the dotted curve for $H^* = 0.6$ T, and $\beta = 90°$ in Fig. 2. The lines for $\beta = 0$ and $\beta = 90$ intersect each other at $E_\parallel^* \simeq 100$ V/cm, 300 and 1,000 V/cm for $H^* = 0.27$ T, 0.6 and 1.31 T, respectively. The dependence of $\bar{\varepsilon}(E_\parallel^*)$ is analogous to the discussed dependence of $\bar{v}^*(E_\parallel^*)$, and the dotted curve is shown also in Fig. 3 for the same H^* and β as in Fig. 2. The only difference is that, due to the intersection of the curves for $\beta = 0$ and $\beta = 90$, they are not so different as in the case of zero magnetic field. As a whole those lines are slightly moved to higher $E_\parallel^*$ (only in the strong magnetic field region of $E_\parallel^*$), when H^* increases, i.e. the magnetic field cools the electrons on average.

The intersections of the lines $\bar{v}^*(E_\parallel^*)$ and $\bar{\varepsilon}(E_\parallel^*)$ for $\beta = 0$ and $\beta = 90$ are connected with the fact that in the strong magnetic field region $(\bar{v}_\perp^* > \bar{v}_\parallel^*)$ the electrons are accelerated mainly in the direction $(\mathbf{E}^* \times \mathbf{H}^*)$ perpendicular to $\mathbf{E}^*$. Electrons, which are moving along the longitudinal axis have a larger probability of APS (Fig. 1). It means that in the strong H^* the current is directed along longitudinal axis when $\beta = 90°$ and it corresponds to the case $\beta = 0$ at $H = 0$.

This is possible to see from Fig. 5, which shows the energy dependence of the anisotropy of the EDF. To calculate it, each energy interval was divided uniformly into 10 intervals for $\cos\theta_1$ and into 10 intervals for ϕ_1 (θ_1 and ϕ_1 are polar and azimutal angles of the momentum $\mathbf{p}^*$).

For $H = 0$ and $\beta = 0$ the EDF is independent on ϕ_1 and depends on θ_1 only. For $H = 0$ and $\beta = 90°$ the dependence of the EDF on θ_1 is shown on Fig. 5 and it is slightly stronger than for $\beta = 0$, because in the last case the electron is accelerated by E^* along the longitudinal axis, where the scattering probability is larger (Fig. 1) and the electrons are cooler (Fig. 3). It $E^* \to 0$, the EDF is isotropic and the frac-

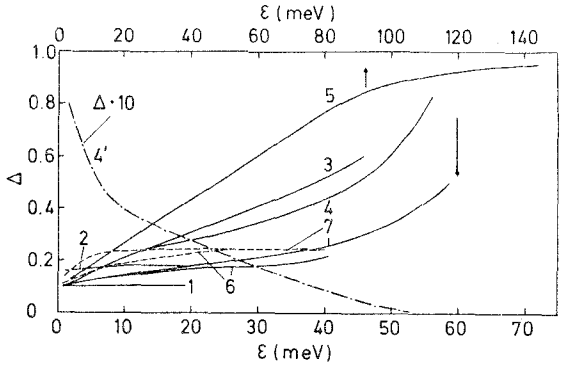

Fig. 5. Energy dependence of the fraction Δ of the electrons, which are in the solid angle 36° with the polar axes, when it directed along $\mathbf{E}^*$ (———), opposite to $\mathbf{E}^*$ (— · — · —) and along the direction $\mathbf{E}^* \times \mathbf{H}^*$ (— — —). $\beta = 90$, E^* and H^* are the same as in Fig. 4

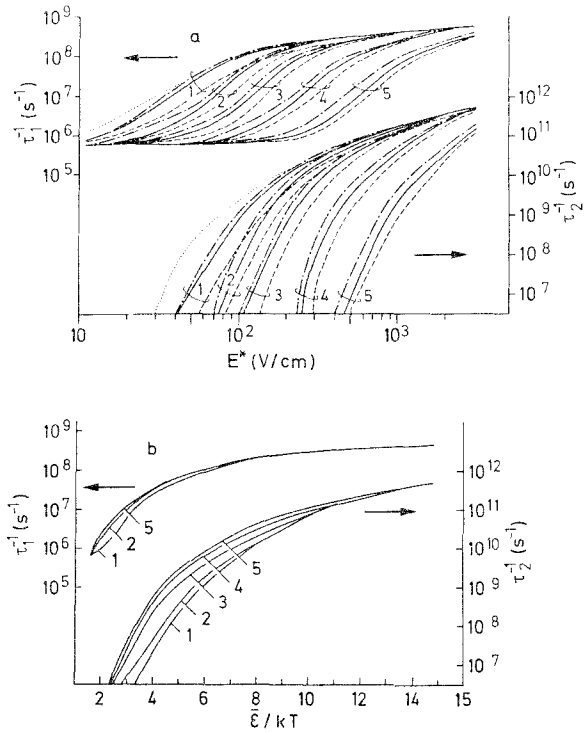

Fig. 6a and b. The dependences of τ_1^{-1} and τ_2^{-1} on E^* **(a)** and on $\bar{\varepsilon}$ **(b)** for the same cases as in Fig. 2

tion of the electrons Δ which lie in the solid angle $\approx 36°$ (i.e. the electrons with θ_1 satisfying $\frac{4}{5} \leqq \cos\theta_1 \leqq 1$ and with only possible ϕ_1) is $\frac{1}{10}$. When E^* increases the EDF is elongated in the direction of $\mathbf{E}^*$. If we choose the polar axis along the direction $\mathbf{E}^*$, then for $E^* = 10$ V/cm $\Delta = 0.16$ and it changes only weakly in the energy range up to 20 meV. For $E^* = 60$ V/cm, 200 and 3,000 V/cm Δ increase when ε increase and for the high E^* almost all electrons of the high energy tail of the EDF are in the narrow solid angle along $\mathbf{E}^*$. The number of electrons with the momentum $\mathbf{p}^*$ opposite to $\mathbf{E}^*$, of course, decrease, when the energy increases, as is shown by the dot-dashed curve in Fig. 5 (this curve represents $\Delta \cdot 10$, because Δ abruptly tends to zero).

For $\beta = 90°$ there is also small anisotropy in ϕ_1. Due to anisotropy of APS the cross section of the EDF by the plane perpendicular to $\mathbf{E}^*$ is an ellipse with the smaller axis along the longitudinal axis of the valley, e.g. for $E^* = 60$ V/cm for energies $\varepsilon < 20$ meV anisotropy in ϕ_1 is about 25%-30%.

If $H \neq 0$ the situation is more complicated. The EDF is of course, isotropic for $E^* \to 0$. In the high E^* region, where the influence of the magnetic field is weak ($\bar{v}_\perp^* < \bar{v}_\parallel^*$), the EDF is elongated along $\mathbf{E}^*$ as in the case of $H = 0$ and the only difference is the anisotropy in ϕ_1, i.e. the electrons have progressed in the direction $\mathbf{E}^* \times \mathbf{H}^*$. In the strong magnetic field region (i.e. in the range of energy, where the opposite to inequality (13) holds) the EDF is elongated in the direction $\mathbf{E}^* \times \mathbf{H}^*$ [see (15, 16)] as it shown by the dashed curves 6 and 7 in Fig. 5. The electrons progress from the $\mathbf{E}^* \times \mathbf{H}^*$ to the $\mathbf{E}^*$ direction when energy increases as is shown by the solid curves 6 and 7 i.e. each energy range in the magnetic field has its own preferential direction of the elongation of the EDF.

Figure 6a shows the field dependence of the intervalley relaxation time describing interaction of electrons with f_1-*phonons* (τ_1^{-1}) and $f_2 + f_3$-phonons (τ_2^{-1}). The τ_1^{-1} has the low electric field limit $\simeq 5.6 \cdot 10^5\ \mathrm{s}^{-1}$ and it increases when E^* increases. The rate of increase of τ_2^{-1} is sufficiently high and also the anisotropy of τ_2^{-1} is considerably larger than τ_1^{-1}. The τ_2^{-1} for $\beta = 0$ and $\beta = 90°$ differs by an order of magnitude and this is the reason the APS anisotropy must take into account to obtain the correct intervalley relaxation time.

The dotted curve in Fig. 6a show the dependence of τ_1^{-1} and τ_2^{-1} on $E_\parallel^*$ as in Fig. 2 for $\beta = 90°$ and $H^* = 0.6$ T. In the low electric field region τ_2^{-1} and τ_1^{-1} are larger than τ_2^{-1} and τ_1^{-1} for $H = 0$. This is caused by the different influence of the magnetic field on electrons with different energies as discussed above.

In the strong H^* the total electric field E^* is considerably larger than $E_\parallel^*$. Figure 7 shows the dependence of the tangent of the angle between E^* and the current ($\mathrm{tg}\beta_2 = \bar{v}_\perp^* / \bar{v}_\parallel^*$) on $E_\parallel^*$. When $E_\parallel^*$ increases, $\mathrm{tg}\beta_2$ decreases. The larger H^* is the more abruptly

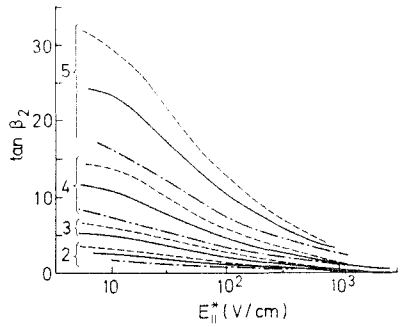

Fig. 7. Dependence of the tangent of the angle between the electric field and the current $\mathrm{tg}\beta_2 = \bar{v}_\perp^*/\bar{v}_\parallel^*$ on the component of the electric field parallel to the current $E_\parallel^*$

$\mathrm{tg}\beta_2$ decreases. The difference between E^* and $E_\parallel^*$ also decreases, as $E_\parallel^*$ increases and at high $E_\parallel^*$ $\mathrm{tg}\beta_2 \to 0$ and $E^* \to E_\parallel^*$. The dependence of $\mathrm{tg}\beta_2$ on the direction of $E_\parallel^*$ is very large for small $E_\parallel^*$.

The mean velocity $\bar{v}^*$ and mean energy $\bar{\varepsilon}$ are determined by the electrons from the energy range in the vicinity of $\bar{\varepsilon}$, where the strong H^* reduces the effect of the total electric field E^*. The intervalley scattering time is determined by high energy electrons. These electrons are effected by the total electric field E^* because for them H^* is weak [see (13)]. Therefore for a given $E_\parallel^*$ we have approximately the same $\bar{v}^*$ and $\bar{\varepsilon}$ for $H^* \neq 0$ but larger τ_1^{-1} and τ_2^{-1} as for $H=0$. This is also seen from Fig. 3. For $\beta = 90°$, $H = 0.6$ T the electric field $E^* = 100$ V/cm corresponds to $E_\parallel^* \simeq 55$ V/cm [see (18) and Fig. 7]. In the low energy range the EDF has a larger slope than for $E^* = 60$ V/cm, $H=0$, but at high energy the slope is smaller. The same holds for $f_0(\varepsilon)$ for $\beta = 0$, $H = 0.6\ T$ and $E^* = 400$ V/cm. This E^* corresponds to $E_\parallel^* \simeq 200$ V/cm and the slope of $\ln f_0(\varepsilon)$ is smaller in the high energy region than for the case $E^* = 200$ V/cm, $H=0$. The smaller slope means that electrons are heated more in this energy range. From Figs. 3 and 6a it is also possible to see that in the magnetic field the declination of τ_1^{-1} from low electric field limit takes place in smaller E^* than the declination of $\bar{\varepsilon}$ from 1.5 kT. For τ_2^{-1} this is seen even more strongly, and it is due to the weakening of H^* with increasing ε.

Figure 6b shows the dependence of τ_1^{-1} and τ_2^{-1} on $\bar{\varepsilon}$. τ_1^{-1} and τ_2^{-1} increase when H^* increases. For τ_1^{-1} this effect is not so large as for τ_2^{-1} because $\hbar\omega_{f_1} \ll \hbar\omega_{f_2}$ and influence of the magnetic field is considerably smaller for $\varepsilon \simeq \hbar\omega_{f_2}$ than for $\varepsilon \simeq \hbar\omega_{f_1}$ (13). Only small changes in τ_1^{-1} are observed for H^* from 0.27 T to 2.87 T because for energies $\varepsilon = \hbar\omega_{f_1}$ the magnetic field $H^* > 0.4$ T is strong. On the other hand τ_2^{-1} increases more than one order of magnitude when H^* increases up to 1.3 T. From $H^* = 1.3$ T to $H^* = 2.87$ there are only small changes in τ_2^{-1}.

The mean energy of electrons is an appropriate parameter to estimate the intervalley relaxation time because for the given H^* the dependence of τ_2^{-1} and τ_1^{-1} on $\bar{\varepsilon}$ change inessentially if β vares from 0° to 90° and they are very close to τ_2^{-1} and τ_1^{-1} of the equivalent isotropic APS approximation. Therefore there is only a solid line for the equivalent isotropic APS in Fig. 6b, for each H^*. The divergences are occur only in two cases. The case $H=0$, $\beta = 90°$ coincides with the equivalent isotropic APS, but for $\beta = 0°$ the result may be presented for τ_2^{-1} as a shift of line 1 in the range of smaller $\bar{\varepsilon}$ on kT/3. Another very small divergence is in τ_1^{-1} for $\beta = 0$ and $\beta = 90°$ for $\bar{\varepsilon} > 9$ kT, but this range is not at all important because then τ_2^{-1} is more than two orders of magnitude greater than τ_1^{-1} and the intervalley scattering time is completely defined by τ_2^{-1}.

τ_2^{-1} can be considered as a parameter characterising the heating of electrons in the high energy tail of the EDF. The larger τ_2^{-1} is the more electrons are in the range $\varepsilon > \hbar\omega_{f_2}$. The dependences of τ_1^{-1} and τ_2^{-1} on $\bar{\varepsilon}$ in Fig. 6b demonstrate that for the same $\bar{\varepsilon}$ the number of electrons in the high energy tail of the distribution function increase considerably as H^* increases.

Let us discuss now the case when **H** is directed along the longitudinal axis of the valley. For the case considered here ($\mathbf{E} \perp \mathbf{H}$) the electric field may only be in the plane perpendicular to this direction, i.e. it is necessary to analyse only the orientation of **E** with $\beta = 90°$.

In the region of high E^* where H^* becomes effectively small (Eq. (13)), the results coincide with the ones presented in Figs. 2–6 for $\beta = 90$. In the range of strong H^* the dependence $\bar{v}_\perp^*(E^*)$ is the same as in Fig. 2 because $\bar{v}_\perp^*$ does not depend on the scattering and on the orientation of the vector $\mathbf{E}^* \times \mathbf{H}^*$ with respect to the principal axes of the valley (17). $\bar{v}_\parallel^*(E^*)$ and $\bar{\varepsilon}(E^*)$ in this region coincide with the case $\beta = 0$ for **H** parallel to the transverse axis of the valley. When E^* increases $\bar{v}_\parallel^*(E^*)$ and $\bar{\varepsilon}(E^*)$ go from the dashed curves to the dot-dashed curves in Fig. 2 and 3 respectively. These transitions from one curve to another lie in the range of E^* where the transition from strong to weak magnetic field occurs for $\varepsilon \simeq \bar{\varepsilon}$.

The results for weak electric field are easy to understand if one uses the momentum relaxation time tensor approximation [15]. In the quasiisotropic approximation for the EDF one has for the mobility

tensor component $\mu_{ii}^{(\alpha)}$ in the principal axes of the valley α the expression [1, 15, 23]:

$$\mu_{ii}^{(\alpha)}=\left\{\frac{2}{3}\int_0^\infty \frac{\varepsilon g(\varepsilon)\tau_{ii}m_i^{-1}(-\partial f_0(\varepsilon)/\partial\varepsilon)d\varepsilon}{1+e^2c^{-2}\tau_t m_t^{-1}(H_1^2\tau_t m_t^{-1}+H_t^2\tau_1 m_1^{-1})}\right\}^{(\alpha)}. \tag{19}$$

Here H_1, H_t and τ_1, τ_t are longitudinal and transverse components of $\mathbf{H}$ and the momentum relaxation time tensor respectively. In the strong magnetic field region unity is small in comparison with the second term in the denominator of (19). Therefore we obtain the same $\bar{v}_\parallel^*$ for both cases, when we calculate $\bar{v}_\parallel^*$ along the longitudinal axis ($\beta=0$) for $H=H_t$ and along transverse axis ($\beta=90°$) for $H=H_1$:

$$\bar{v}_\parallel^*=\frac{2c^2E^*}{3e^2H^{*2}}\left\{\int_0^\infty \frac{\varepsilon g(\varepsilon)}{\tau_\perp}\left(-\frac{\partial f_0(\varepsilon)}{\partial\varepsilon}\right)d\varepsilon\right\}^{(\alpha)}. \tag{20}$$

The dependences $\tau_1^{-1}(E^*)$ and $\tau_2^{-1}(E^*)$ also change from the dashed curves to the dot-dashed curves in the range of E^* where H^* is effectively intermediate. The dependences $\tau_1^{-1}(\bar{\varepsilon})$ and $\tau_2^{-1}(\bar{\varepsilon})$ for this orientation of $\mathbf{H}$ are the same as for the previously considered case of $\mathbf{H}$ along the transverse axis of the valley (Fig. 6b), i.e. $\bar{\varepsilon}$ is a good parameter to characterise τ for only orientation of $\mathbf{E}^*$ and $\mathbf{H}^*$.

In conclusion it is necessary to stress that in many-valley semiconductors the most interesting phenomena involve the intervalley redistribution of electrons [1, 2, 9, 10, 12]. In the present calculation it is shown that the intervalley scattering time changes by an order of magnitude under the rotation of $\mathbf{E}^*$ or $\mathbf{H}^*$ from longitudinal to transverse axes of the valley. Therefore the intervalley redistribution of the electrons differs considerably when APS anisotropy taken into account compared to case when equivalent isotropic APS is introduced.

I would like to thank Prof. P. Fulde for friendly support and the possibility of completing this work in his department.
The author is also grateful to Dr. E. Göbel, Dr. J. Samson and Dr. G. Huggins for their critical reading of the manuskript.

Appendix

We given here an example of how to use the plots presented in this paper to derive the current-voltage and other characteristics of n-Si.

The electron concentration n_α in the valley α may be calculated from the simple equation [1, 2]

$$n_\alpha=n\tau_\alpha\Big/\sum_{\beta=1}^{\lambda}\tau_\beta,\qquad \alpha=1\ldots\lambda, \tag{A1}$$

where τ_α is the intervalley scattering time in the valley α. All characteristics of the many-valley semiconductor are the sums over the valleys, i.e. the mean drift velocity, $\mathbf{v}_d$, the mean energy, $\bar{\varepsilon}$, (and so on) are:

$$\mathbf{v}_d=\sum_{\alpha=1}^{\lambda}\bar{\mathbf{v}}_\alpha\tau_\alpha\Big/\sum_{\alpha=1}^{\lambda}\tau_\alpha,\qquad \bar{\varepsilon}=\sum_{\alpha=1}^{\lambda}\bar{\varepsilon}_\alpha\tau_\alpha\Big/\sum_{\alpha=1}^{\lambda}\tau_\alpha, \tag{A2}$$

where $\mathbf{v}_\alpha$ and $\bar{\varepsilon}_\alpha$ are the mean velocity and mean energy in the valley α. τ_α, $\bar{\mathbf{v}}_\alpha$, $\bar{\varepsilon}_\alpha$ depend only on the effective electric, $\mathbf{E}_\alpha^*$, and magnetic, $\mathbf{H}_\alpha^*$, fields in a valley α. Equation (7) define $\mathbf{E}_\alpha^*$ and $\mathbf{H}_\alpha^*$ in terms of the total electric $\mathbf{E}$ and magnetic $\mathbf{H}$ fields. $\mathbf{H}$ is the external field and $\mathbf{E}$ must be calculated subjected to the condition that the component j_{tr} of the current $\mathbf{j}$ transverse to the longitudinal axis of the sample vanishes.

$$j_{\mathrm{tr}}=en\cdot v_{d,\mathrm{tr}}=0. \tag{A3}$$

Let us consider case of a sample cut so that the current $\mathbf{j}$ is along [100] (x-axis) and the transverse magnetic field is along [001] (z-axis). Due to the symmetry, the total electric field $\mathbf{E}$ has two components:

$E_x=E\cos\gamma$ (the applied component E_p) and
$E_y=E\sin\gamma$ (the transverse component, due to the magnetic field and intervalley redistribution), where γ is the angle between $\mathbf{j}$ and $\mathbf{E}$.

From Eq. (7) for the non zero components of the effective fields $\mathbf{E}_\alpha^*$ and $\mathbf{H}_\alpha^*$ we have

$$\begin{aligned}
&E_{x,1}^*=E(m/m_1)^{\frac{1}{2}}\cos\gamma;\\
&E_{y,1}^*=E(m/m_t)^{\frac{1}{2}}\sin\gamma;\qquad H_{z,1}^*=Hm/(m_tm_1)^{\frac{1}{2}}\\
&E_{x,2}^*=E(m/m_t)^{\frac{1}{2}}\cos\gamma;\\
&E_{y,2}^*=E(m/m_1)^{\frac{1}{2}}\sin\gamma;\qquad H_{z,2}^*=Hm/(m_tm_1)^{\frac{1}{2}}\\
&E_{x,3}^*=E(m/m_t)^{\frac{1}{2}}\cos\gamma;\\
&E_{y,3}^*=E(m/m_t)^{\frac{1}{2}}\sin\gamma;\qquad H_{z,3}^*=Hm/m_t.
\end{aligned} \tag{A4}$$

Here the pair of valleys on [100], [010] and [001] axes are denoted as a valley number 1, 2 and 3, respectively. The angle γ is zero if $H=0$. The effective fields and currents in each valley coincide with x-axis. Equation (A3) is satisfied automatically. The total field E coincides with the applied field E_p. The E_α is defined in each valley [see (A4)] for a given E_p. The drift velocity is simply calculated by summation in (A2), taking into account the dependences of v_α and τ_α on E_α shown in Fig. 2 and 6a. The result is shown in Fig. 8 for two different cases when APS is treated as anisotropic scattering (solid curve) and as effective isotropic scattering (dot-dashed curve). The current-voltage characteristics ($j=env_d$)

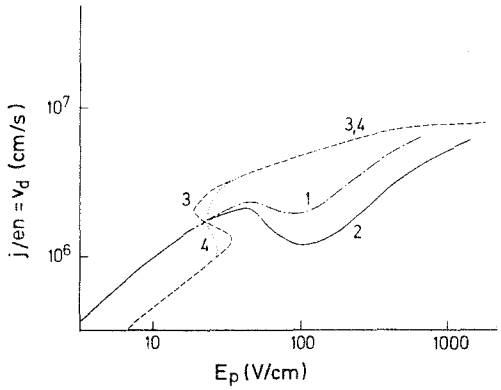

Fig. 8. Dependence of the drift velocity, v_d, (or current density per electron, $j/en = v_d$) on the applied electric field, E_p, in n-Si at 27 K for $\mathbf{j} \parallel [100]$ and $\mathbf{H} \parallel [001]$: 1, 2 – $H = 0$, 3 – $H = 0.775$ T, 4 – $H = 1.7$ T. 1 – calculation using equivalent isotropic APS and 2–4-ansisotropic APS

has N-type negative differential conductivity ($N-ndc$), which has previously been studied theoretically and experimentally (see e.g. [24, 11]). If the anisotropy of APS is taken into account, the absolute value of the $N-ndc$ is larger and current is smaller in a high electric field, when the electrons are in the cold valley where the APS is larger.

The problem is not really more complicated in the presence of a magnetic field. The only difference is that both components ($v_\parallel^*$ and $v_\perp^*$) of the mean velocity in each valley are present in (A2) and the dependences of $\bar{\mathbf{v}}^*$ and τ_α on E_α must be taken from Fig. 2 and 6a for the appropriate H_α^*.

The value of the total electric field $\mathbf{E}$ is taken as given. γ is adjusted until Eq. (A3) is satisfied. (The vector $\mathbf{v}$ [Eq. (A2)] rotates when γ changes). The effective fields E_α are defined at each step. The transverse ($E_y = E \cdot \sin\gamma$) and applied ($E_p = E \cdot \cos\gamma$) components of the electric field, the drift velocity v_d (and so on) are also defined, when the correct angle γ s found.

Current-voltage characteristics are shown in Fig. 8 for two values of the magnetic field ($H = 0.775$ T and $H = 1.7$ T). These display $S-ndc$. In a strong magnetic field $\mathbf{E}$ is close to the y-axis (γ is close to $\pi/2$). The hottest valley is the first one, where H_1^* is small but E_1^* is large [see (A4)]. Due to repopulation of electrons in two cold valleys, the ratio E_y/E_p increases faster than E, when E increases. That is why E_p decreases when E increases in a certain region of E. More detailed discussion of $S-ndc$ and the experimental results can be found in [14, 23, 24]. The magnetoresistance in a small magnetic field and the range of electric field with $S-ndc$ increase, but the absolute value of the ndc decreases when the anisotropy of the APS is taken into account as in Fig. 8.

The dependence of $\bar{\varepsilon}$ on E_p is also N-type for $H = 0$ and S-type in strong magnetic field.

Additional intervalley scattering at an impurity is ordinarily taken into account at low temperatures [12–14]. Its probability, τ_0^{-1}, is taken as field-independent. The current-voltage characteristics have well developed N- and $S-ndc$ for τ_0^{-1} in the range 10^7–$10^9\,s^{-1}$. We choose $\tau_0^{-1} = 10^8\,s^{-1}$ in Fig. 8, as has previously been done for the effective isotropic APS [12–14].

References

1. Conwell, E.M.: High field transport in semiconductors. New York: Academic Press 1967
2. Dienys, V., Pozela, J.: Gorjatschie electroni. Vilnius. Mintis (1971)
3. Shannon, J.M.: In: Solid state devices 1983. Inst. Phys. Conf. Ser. N°. 69, 45 (1984)
4. Balk, P.: In: Solid State Devices 1983, Inst. Phys. Conf. Ser. N°. 69, 63 (1984)
5. Ferry, D.K.: J. Phys. (Paris) Colloq. C7, Suppl. 10, T42, pp. C7-253 (1981)
6. Barker, J.R., Ferry, D.K.: Solid State Electron. **23**, 519, 531, 545 (1980)
7. Kurosawa, T.: J. Phys. Soc. Jpn. Suppl. **21**, 424 (1966)
8. Fawcett, W., Bordmann, D.A., Swain, S.: J. Phys. Chem. Solids **31**, 1963 (1970)
9. Canali, C., Jacoboni, C., Nava, F., Ottaviani, G., Alberigi-Quaranta, A.: Phys. Rev. B**12**, 2265 (1975)
10. Jacoboni, C., Regiani, L.: Rev. Mod. Phys. **55**, 645 (1983)
11. Jørgensen, M.H., Gram, N.O., Meyer, N.J.: Solid State Commun. **10**, 337 (1972)
12. Asche, M., Gribnikov, Z.S., Ivaschenko, V.M., Kostial, M., Mitin, V.V., Sarbei, O.G.: Zh. Eksp. Teor. Fiz. **81**, 1347 (1981) (Sov. Phys. JETP **54**, 715 (1981))
13. Gribnikov, Z.S., Ivaschenko, V.M., Mitin, V.V., Sarbei, O.G.: Preprint N°. 8, Institute of Physics, Academy of Sciences of the Ukrainian SSR, Kiev 1981
14. Ivaschenko, V.M., Mitin, V.V.: Ukr. Fiz. Zh. **29**, 123 (1984)
15. Herring, C., Vogt, E.: Phys. Rev. **101**, 944 (1956)
16. Jørgensen, M.H.: Phys. Rev. B**18**, 5657 (1978)
17. Bir, G.L., Pikus, G.E.: Symmetry and strain-induced effects in semiconductors. p. 350. New York: Wiley 1975
18. Baranski, P.I., Klochkov, V.L., Potykevich, I.V.: Poluprovodnikovaya Electronika (Svoistva materialov), Spravochnik. Kiev: Naukova dumka 1975
19. Handbook of Chemistry and Physics. 60th Edn. p. E.-106. Boca Raton, Florida: CRC Press, Inc. 1981
20. Mitin, V.V.: Fiz. Tekh. Poluprovodn. **17**, 325 (1983) (Sov. Phys. Semicond. **17**, 205 (1983))
21. Price, P.J.: Semicond. Semimetals **14**, 249 (1979)
22. Asche, M., Kostial, H., Sarbei, O.G.: Phys. Status Solidi (b) **91**, 521 (1979)
23. Mitin, V.V.: Phys. Status Solidi (b) **49**, 125 (1972)
24. Sarbey, O.G., Kurtenok, L.F., Movchan, E.A., Mitin, V.V.: Inst. Phys. Conf. Ser., 1979. No. 43, Chap. 10, p. 339

V.V. Mitin
Max-Planck-Institut
für Festkörperforschung
Heisenbergstrasse 1
D-7000 Stuttgart 80
Federal Republic of Germany

R. N. Bhatt and T. M. Rice, Phys. Rev. B 23, 1920 (1981)
A similar principle has been discussed for the case of correlated hopping of carriers in terms of an increase in the effective "hopping length", e.g. in reference 3.
A. S. Skal, B. I. Shklovskii, and A. L. Efros, Sov. Phys.- JETP Lett. 17, 377 (1973)

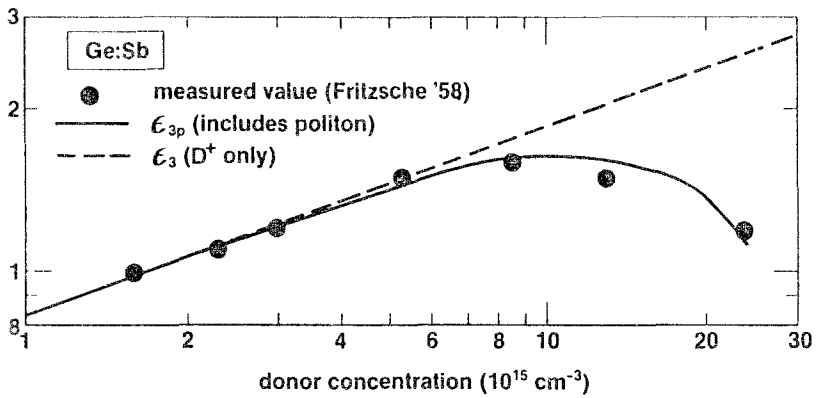

Fig. 1. Activation energies for impurity hopping conduction in Ge:Sb. The dashed line for ϵ_3 is a least squares fit to the low N_D data[2]. The solid line for ϵ_{3P} is obtained from Eq. 5.

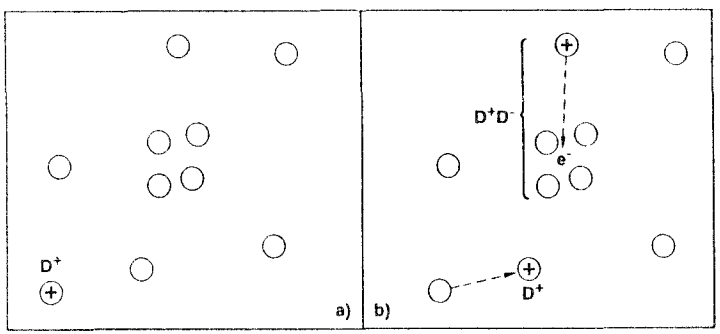

Fig. 2. Schematic representation of politon formation. The circles denote donor impurities. (a) Before the D^+ hops (b) The hop of the D^+ is accompanied by the creation of a D^+D^- resulting in a politon comprised of the D^+ and D^+D^- with lower energy than the bare D^+.

18 Intern. Conf. in Semicon, Stockholm 1986.

PHENOMENA UNDER COOLING OF CARRIERS IN THE ELECTRIC FIELD

V. V. Mitin and N. A. Zakhleniuk

Institute of Semiconductors of the Ukrainian Academy of Sciences, Kiev-28, Pr. Nauki, 115
USSR

ABSTRACT

The decrease of the current due to freezing out of the carriers caused by the electric field is predicted. The phenomena under cooling of the carriers by the electric field in many-valley semiconductor is also discussed.

1. INTRODUCTION. WHAT IS THE COOLING?

We are dealing with doped germanium-like semiconductors. The probability of the emission of the optical phonon $W_o(\varepsilon > \hbar\omega_o)$ is much greater than the probability of any other scattering process $W_a(\varepsilon > \hbar\omega_o)$ if the energy ε of a charge carrier exceeds the energy $\hbar\omega_o$ of this phonon. The low temperature case ($kT \ll \hbar\omega_o$) is treated only. The mean energy of the carriers $\bar{\varepsilon}$ increases up to the electric field $E \leq E_c$ only, as shown by curve 1 in Fig. 1. The emission of optical phonon becomes essential for $E \geq E_c$ (e.g. E_c=4.4 V/cm for N_i=10^{12} cm^{-3} and E_c=15.7 V/cm for N_i=10^{14} cm^{-3} in p-Ge at 4 K). Therefore the carriers flow from high-energy to low energy region. They remain in this region due to the intensive elastic impurity scattering. As a result, $\bar{\varepsilon}$ decreases with increasing E for $E > E_c$ (curve 1 in Fig. 1). This cooling effect was predicted theoretically [1] and observed experimentally [2]. The cooling take place